Enhanced absorption and carrier collection in Si wire arrays for photovoltaic applications

Michael D. Kelzenberg, Shannon W. Boettcher, Jan A. Petykiewicz, Daniel B. Turner-Evans, Morgan C. Putnam, Emily L. Warren, Joshua M. Spurgeon, Ryan M. Briggs, Nathan S. Lewis and Harry A. Atwater*

Si wire arrays are a promising architecture for solar-energy-harvesting applications, and may offer a mechanically flexible alternative to Si wafers for photovoltaics[1-17]. To achieve competitive conversion efficiencies, the wires must absorb sunlight over a broad range of wavelengths and incidence angles, despite occupying only a modest fraction of the array's volume. Here, we show that arrays having less than 5% areal fraction of wires can achieve up to 96% peak absorption, and that they can absorb up to 85% of day-integrated, above-bandgap direct sunlight. In fact, these arrays show enhanced near-infrared absorption, which allows their overall sunlight absorption to exceed the ray-optics light-trapping absorption limit[18] for an equivalent volume of randomly textured planar Si, over a broad range of incidence angles. We furthermore demonstrate that the light absorbed by Si wire arrays can be collected with a peak external quantum efficiency of 0.89, and that they show broadband, near-unity internal quantum efficiency for carrier collection through a radial semiconductor/liquid junction at the surface of each wire. The observed absorption enhancement and collection efficiency enable a cell geometry that not only uses 1/100th the material of traditional wafer-based devices, but also may offer increased photovoltaic efficiency owing to an effective optical concentration of up to 20 times.

Arrays of Si wires with radial p–n junctions are being explored as an alternative to wafer-based Si geometries for photovoltaic applications[1-6]. The radial collection geometry can, in principle, tolerate the use of low-purity Si with a short minority carrier diffusion length, while allowing for high solar-energy-conversion efficiencies, by providing a short minority carrier collection path equal to the wire radius. Large-area arrays of Si wires can be grown on commonly available (for example, glass[4,5]) or re-usable[17] substrates using the vapour–liquid–solid (VLS) growth process[19]. Oriented horizontally, single-nanowire solar cells grown by the VLS process have demonstrated up to 3.4% conversion efficiency[13]. Si nanowire arrays have also been shown to have beneficial optical absorption properties for photovoltaic applications, owing to the subwavelength scale of the wires[4-12].

Obtaining optimal solar-energy-conversion efficiencies for macroscopic wire-array devices, however, requires not only that the wire array provide effective absorption of the photons incident onto the entire device—at a variety of wavelengths and angles of incidence—but also that the wires be optimally sized for efficient carrier collection. A theoretical treatment of radial p–n junctions[1] predicts optimal efficiency for wires that have a diameter of the order of the minority-carrier diffusion length, which is
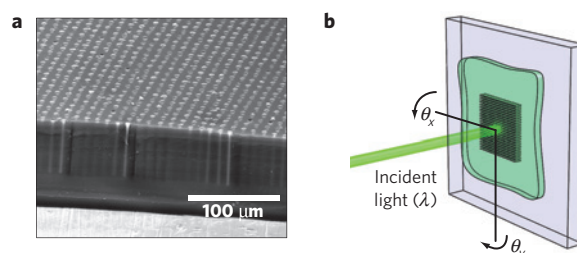

Figure 1 | Structure of Si wire arrays prepared for optical measurements. a, SEM image of a peeled-off, polymer-embedded wire array, viewed upside-down (at 60° tilt) to illustrate the order and fidelity of the embedded wires. **b**, Schematic of the illumination conditions and definition of the incidence angles θ_x and θ_y.

2–10 μm for our VLS-grown Si wires[20,21]. On the basis of these diffusion lengths, micrometre-scale-diameter single-wire solar cells have been predicted to achieve over 17% conversion efficiency[22]. This framework motivates the study of the optical absorption of Si microwire arrays, as these structures will interact with light differently from the subwavelength structures previously studied. We report herein the design, implementation and demonstration of Si microwire-array devices that show, over macroscopic device areas, effective incident light absorption as well as efficient charge-carrier collection.

To study the optical absorption of Si wire arrays independently from the optical effects of the growth substrate, the arrays were grown by a photolithographically patterned VLS process[23], then embedded in the transparent polymer polydimethylsiloxane (PDMS) and peeled intact from the growth wafer as flexible films[16] (Fig. 1a). These films were well suited for optical transmission and reflection measurements, which were carried out using an integrating sphere, as a function of wavelength and incidence angle (Fig. 1b). Numerous high-fidelity arrays of varying wire length, diameter, spacing and tiling patterns (including periodic, quasi-periodic and random motifs) were investigated in this fashion. The areal wire packing fractions, η_f, ranged from 1.6 to 16%. Figure 2 shows an example wire array of each of the seven investigated tiling patterns (top rows). Following peel-off, the transmitted optical diffraction patterns (third row) were used to orient the wire lattice patterns relative to the tilt directions (θ_x, θ_y), and angularly resolved transmission measurements were carried out (bottom row).

Owing to the vertical orientation of the wires, all of the arrays showed lower absorption at normal incidence ($\theta_{x,y} = 0°$) than at other angles. The well-aligned rows and columns of
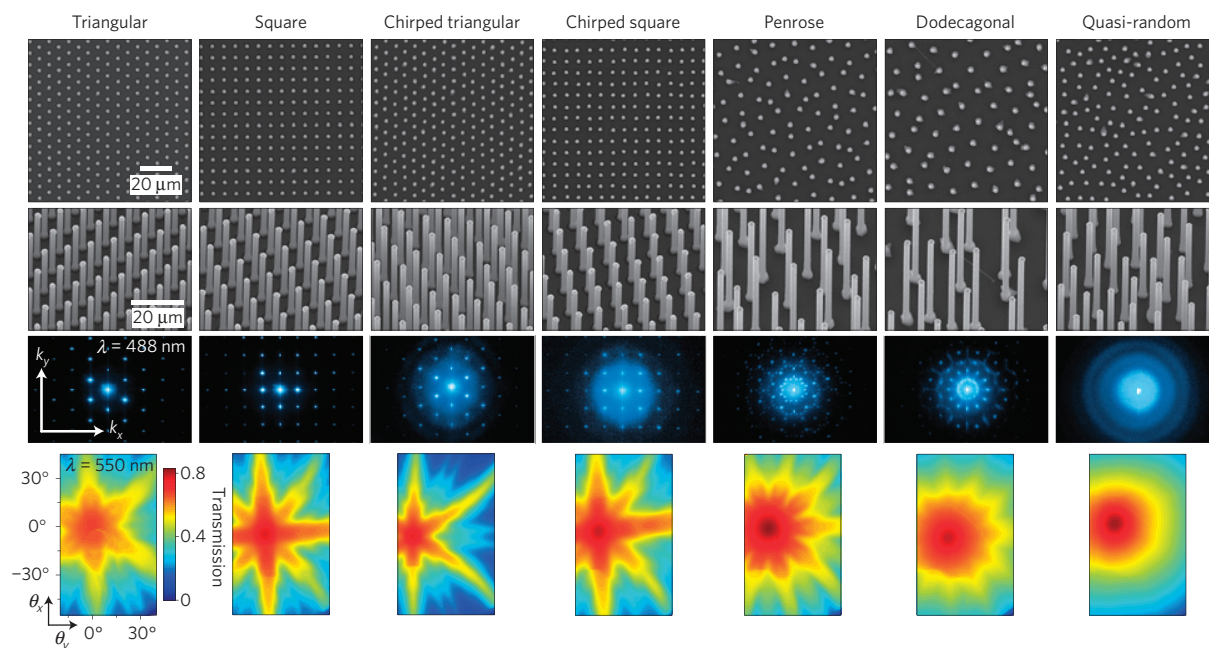
Figure 2 | Representative composition and optical properties of each wire-array tiling pattern. The scale bars in the left column apply to all images across each row. Top row: SEM images of as-grown wire arrays viewed from a top-down perspective. Second row: SEM images viewed at a 20° angle. Third row: Transmitted diffraction patterns of polymer-embedded wire arrays on a quartz slide, observed at $\lambda = 488$ nm. The axes indicate 4,000 cm^{-1} in the direction of k_x and k_y. Bottom row: Integrated transmission of each wire array observed at $\lambda = 550$ nm as a function of the beam incidence angle (θ_x, θ_y).

wires produced by periodic arrangements led to greater areal packing fractions (and thus higher overall optical absorption) than were obtained by quasi-periodic or random arrangements. However, the periodic arrangements also showed a strongly anisotropic angular absorption profile, which would produce low-absorbing 'dead spots' in a photovoltaic device. Alteration of the VLS catalyst template pattern to produce mild randomization (chirping) of the wire position within the periodic arrays was not sufficient to eliminate the obvious optical absorption minima at certain angles of incidence. Furthermore, increasing the areal packing fraction of the wire arrays to $\eta_f > 12\%$ increased their reflectivity, presumably because of the increasing area of the reflective Si/PDMS dielectric interface at the top of each wire, which in turn reduced their overall absorption (see Supplementary Information). These observations suggested that, for Si wire arrays to achieve maximal absorption over the relevant wavelengths and incidence angles of solar illumination, the reflectivity of the Si surfaces must be reduced, and the light passing between the wires must be randomized.

Figure 3 demonstrates the light-trapping techniques that were used to maximize the absorption of a square-tiled array of 67-μm-long Si wires. With an areal packing fraction of $\eta_f = 4.2\%$, this array contained the same volume of Si as a 2.8-μm-thick planar sheet of Si. As expected, the peak absorption was relatively low at normal incidence (<0.5) and increased at steeper angles of incidence (Fig. 3a). The wire array was then placed on a mirror-like Ag back-reflector (Fig. 3b), to emulate a metal back contact to a prototypical wire-array solar cell, as well as to increase the optical path length within the array. Although this step substantially increased the absorption of the array (approaching peak normal-incidence values of 0.8), the normal-incidence absorption remained significantly weaker than that at off-normal-incidence angles. To further improve absorption, two more light-trapping measures were implemented on a different portion of the wire array. Before being embedded in PDMS, a SiN$_x$ antireflective coating (80 nm nominal thickness) was conformally deposited onto the tops and sides of these wires (Supplementary Fig. S1). In addition, Al$_2$O$_3$

particles (0.9 μm nominal diameter) were added to the PDMS infill, to scatter the light that might otherwise pass between the wires (Supplementary Fig. S3). These materials were chosen because they have negligible absorption across the wavelengths studied here (Supplementary Figs S2,S4), and thus enabled the direct observation of absorption enhancement within the Si wires themselves. As shown in Fig. 3c, these light-trapping measures virtually eliminated the angular sensitivity of the wire array's absorption, and increased the peak normal-incidence absorption to 0.92. When placed on a Ag back-reflector, the array's peak absorption increased to 0.96 (Fig. 3d), which is nearly the maximal absorption achievable by any material fully embedded within PDMS (owing to the ~3% reflectivity of the PDMS–air dielectric interface.)

To provide a figure of merit for the absorption measurements, the overall fraction of above-bandgap photons that each wire array would absorb throughout a day of operation as a non-tracking solar cell, A_{avg}, was calculated on the basis of a time-resolved reference spectrum of direct solar insolation[24] in conjunction with the measured angle- and wavelength-dependent absorption values of the wire arrays (Supplementary Fig. S10). Figure 3e shows the A_{avg} calculations that correspond to the absorption measurements shown in Fig. 3a–d. Also shown, for comparison, is the A_{avg} calculation that corresponds to the measured absorption of a commercial, 280-μm-thick polycrystalline Si solar cell with a dielectric antireflective coating. The optimal Si wire array showed $A_{avg} = 0.85$, which although slightly below that of the commercial Si solar cell ($A_{avg} = 0.87$), is remarkable considering that this wire-array film contained ~1% as much Si (per specimen area) as the commercial solar cell. This volume reduction implies substantial optical concentration within the Si wires.

To further gauge the absorption enhancement of the wire-array geometry, the measured absorption, $A_{WA}(\theta_x, \lambda)$, of the optimal wire array from Fig. 3d was compared with the theoretical absorption limits of a 2.8 μm planar Si absorber, which contains the same average volume of Si per unit area as the wire array (Fig. 4). On the basis of bulk Si properties[25] and neglecting interference
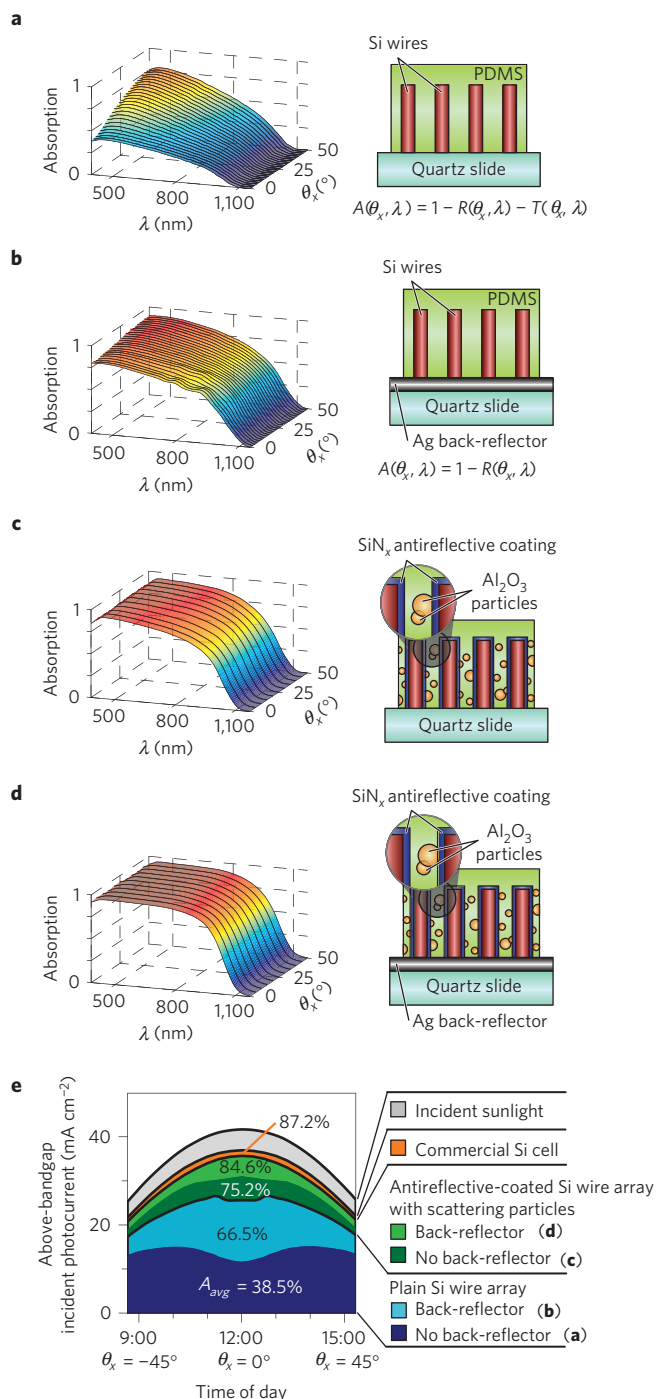
Figure 3 | Light-trapping techniques and figure of merit (A_{avg}) calculation. a,b, Schematic and measured absorption of a $\eta_f = 4.2\%$ square-tiled wire array on a quartz slide (**a**) and on a Ag back-reflector (**b**). **c,d,** Schematic and measured absorption of this array with an antireflective coating and embedded light-scatterers, measured on a quartz slide (**c**) and on a Ag back-reflector (**d**). **e,** A plot of A_{avg} calculations corresponding to each absorption measurement shown in **a–d**, showing the incident sunlight and spectrally weighted absorption of each throughout the day, compared with the measured absorption of a commercial, antireflective-coated, polycrystalline Si solar cell.
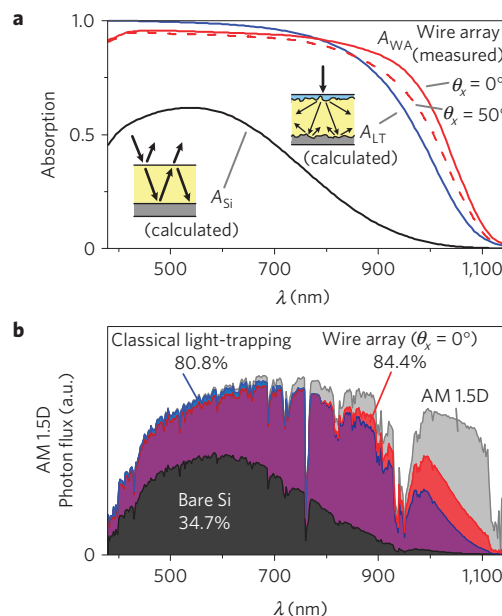
Figure 4 | Measured Si wire-array absorption versus theoretical absorption of an equivalently thick, planar Si absorber. a, Measured absorption (A_{WA}, red) of the Si wire array from Fig. 3d (which had an equivalent planar Si thickness of 2.8 μm), at normal (solid) and 50° (dashed) incidence, versus the calculated normal-incidence absorption of a 2.8-μm-thick planar Si absorber, with an ideal back-reflector, assuming: bare, non-texturized surfaces (A_{Si}, black) and ideally light-trapping, randomly textured surfaces (A_{LT}, blue). **b,** Illustration of the normal-incidence, spectrally weighted absorption of the AM 1.5D reference spectrum, corresponding to each of the three absorption cases plotted above.

the 'ergodic limit', is the maximally achievable absorption (in the ray-optic limit) of a planar-sheet absorber that uses ideally random (for example, Lambertian) light-trapping[18,26].

As shown in Fig. 4a, the wire array's absorption exceeded the planar light-trapping limit for infrared wavelengths ($\lambda > 800$ nm). This behaviour exemplifies a useful property of microstructured, non-planar absorber geometries (including wire arrays), in that they can achieve greater absorption per material volume than achievable by a randomly textured, planar-sheet absorber geometry. This effect has been described, through use of a statistical ray optics model, for idealized films of polymer-embedded Si granules[26], and has also been simulated for Si wire arrays[3,9]. Figure 4b shows, using the AM 1.5D spectrum at normal incidence, that the enhanced infrared absorption of the Si wire array yielded a greater overall absorption of above-bandgap photons than the equivalently thick, ideally light-trapping planar absorber. In fact, taking all measured incidence angles into account, the day-integrated absorption of the wire array ($A_{avg} = 0.85$) slightly exceeded that of the planar light-trapping case ($A_{avg} = 0.82$). Thus, the Si wire-array geometry can enable solar cells that reach, and potentially even exceed, the theoretical absorption limit, per volume of Si, of ideal light-trapping within a conventional planar geometry.

The enhanced absorption properties of Si wire arrays enable high quantum efficiencies for photovoltaic applications. To demonstrate this, a photoelectrochemical cell (Fig. 5a) was used to measure the external quantum efficiency (EQE) of Si wire-array photoelectrodes, which consisted of p-type wire arrays grown on degenerately doped (and thus photovoltaically inactive, see Supplementary Fig. S15) Si wafers. The transparent electrolyte formed a rectifying junction to the top and sides of each wire (analogous to a radial p–n junction[27]), enabling photoelectrochemical characterization of the

effects, two theoretical absorption limits were calculated for the equivalently thick Si slab: A_{Si}, which results from the use of bare, non-textured Si surfaces (black), and A_{LT}, which results from ideal classical light-trapping at the Si surfaces (blue). The latter case,

angle- and wavelength-dependent EQE of the wire-array electrode. However, because the wires were immersed in an electrolyte and attached to their growth substrate, this technique did not permit the use of a polymer infill, a dielectric antireflective coating and/or a planar metal back-reflector. Thus, relatively long (130 μm) and sparse ($\eta_f = 6.2\%$) square-tiled wire arrays were grown, to minimize the transmission of light into the photovoltaically inactive growth substrate while also minimizing the area of the reflective top surface of the Si wires (Fig. 5b, upper left). This geometry yielded up to 0.85 peak EQE (lower left), but suffered from substantially reduced EQE at normal incidence (centre left). Evaluating the EQE across the day-integrated solar spectrum (as carried out for A_{avg} above) yielded $EQE_{avg} = 0.56$ (Supplementary Fig. S19). When Al_2O_3 light-scattering particles were drop-cast into this wire array (Fig. 5b, upper right), the normal-incidence 'dead spot' was virtually eliminated (centre right), the peak EQE increased to 0.89 (lower right) and the day-integrated EQE_{avg} increased to 0.68. This value is significant, considering that the photoelectrochemical cell configuration precluded the use of a metal back-reflector or an antireflective coating, both of which are known to substantially improve the optical absorption (Fig. 3), and both of which could be used within a solid-state, radial p–n junction wire-array solar cell. Thus, the results presented here represent lower bounds, rather than upper limits, on the EQE that could be achieved by use of the Si wire-array geometry.

A particular concern for photovoltaic applications of VLS-grown wire arrays is the possibility of parasitic absorption, which could be caused by the presence of surface states, impurities or residual VLS catalyst metal deposits[28]. To determine the extent of useful (that is, non-parasitic) absorption, the internal quantum efficiency (IQE) of the Si wire-array electrodes was determined by normalizing their measured EQE to their measured absorption. To mitigate difficulties in peeling the Al_2O_3 particles intact with the array described above, this measurement was carried out on less-densely packed ($\eta_f = 3.0\%$) arrays of shorter (90 μm) wires without light-scatterers (Fig. 5c, inset). Figure 5c compares the measured normal-incidence EQE of this wire-array electrode (blue) to the measured normal-incidence absorption of the wires after being polymer-embedded and peeled from the growth substrate (black). Owing to the similarity between these illumination conditions (for example, the similar refractive indices of the surrounding PDMS/electrolyte solution, see Supplementary Information), this comparison was used to determine the approximate IQE of the wire-array electrode (red). The IQE exceeded 0.9 for most above-bandgap photon energies ($\lambda = 400$–900 nm), in good agreement with radial junction theory, which predicts a near-unity IQE for any wire having a radius of less than the minority carrier diffusion length[1,3]. Although the reported IQE decreased for $\lambda > 900$ nm, the measured absorption nevertheless differed from the measured EQE by no more than 0.05 throughout the entire measurement range, confirming that the absorption was predominately non-parasitic, while also providing a compelling demonstration of the broadband, near-unity IQE expected for a radial-junction, Si wire-array photovoltaic device.

The observed absorption enhancement and collection efficiency suggest that Si wire-array solar cells can benefit from the well-known improvements in open-circuit voltage (and thus photo-voltaic efficiency) that are achievable under optical concentration[29]. When sunlight illuminates a wire array, the absorption is laterally confined within the relatively small cross-sectional area of the wires. In this regard, the $\eta_f = 4.2\%$ wire array that showed $A_{avg} = 0.85$ can be considered, to first order, as a ×24 lateral geometric concentrator that achieved a ×20 average intensity concentration without the use of conventional focusing optics. Several theoretical studies have discussed the enhanced photogeneration rates in wire-array absorbers[3,9,30].
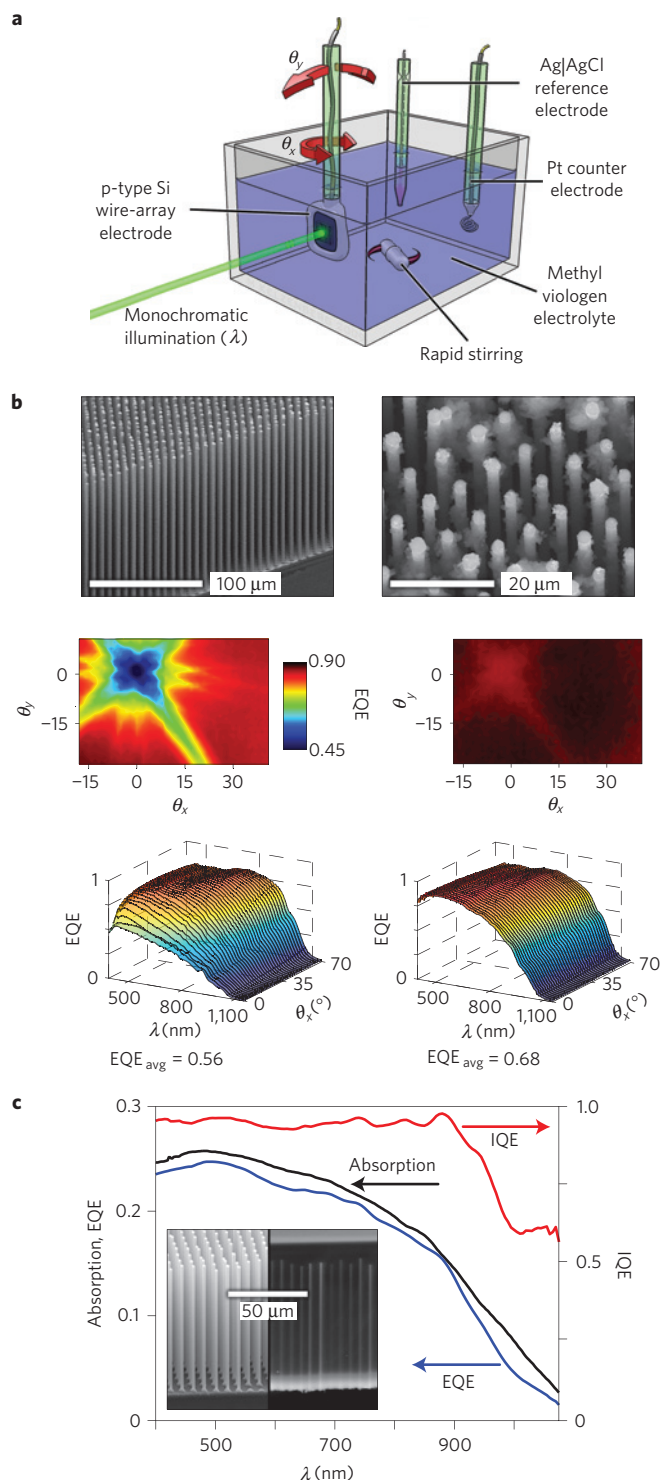

Figure 5 | Photoelectrochemical characterization of Si wire arrays.
a, Schematic of the photoelectrochemical cell and definition of illumination angles. **b**, Effect of light-scattering particles on wire-array electrode EQE. Top: SEM image; centre: two-dimensional angle-resolved EQE at $\lambda = 550$ nm; bottom: wavelength-angle-resolved EQE at $\theta_y = 0°$, of a Si wire-array electrode without (left) and with (right) Al_2O_3 light-scattering particles. **c**, Normal-incidence absorption measurement of a polymer-embedded wire array (black) and normal-incidence EQE of a wire-array electrode (blue). A 50 nm running average was applied to the absorption, to reduce interference fringes in the experimental data. The resulting IQE is plotted in red. Inset: SEM images of the wire-array electrode (left) and the polymer-embedded wire array (right).

We have experimentally demonstrated that Si wire arrays have advantageous optical properties for photovoltaic applications, including reasonable absorption of sunlight despite low areal packing fractions, extended near-infrared absorption compared with planar-sheet absorbers and effective optical concentration over a wide range of incidence angles. We note that the observations reported herein are not limited to Si wire-array solar cells. The wire-array geometry, along with other microstructured, non-planar absorber geometries (for example, the microcell geometry[31] or CdS/CdTe nanopillars[32]), offers opportunities to manipulate the ratio of illumination area to absorption volume, and may be useful in improving the efficiency or reducing the materials consumption of many photovoltaic technologies.

Methods

Wire-array fabrication. Si wire arrays were grown by a photolithographically patterned VLS process as described previously[23]. Wires were grown on p-type ⟨111⟩ Si wafers ($\rho < 0.001\,\Omega\,cm$), using a 300 nm thermal oxide for catalyst confinement and evaporated Au, Cu or Ni (400–700 nm thickness) as the VLS catalyst. No notable differences were observed between the optical properties of wires grown using Au, Cu or Ni catalyst metal. Following growth, the wire arrays were etched in 5% HF(aq) for 30 s. To remove the catalyst metal, Au-catalysed wires were then etched for 30 min in a solution of 9:1 Gold Etchant TFA (Transene) to 36% HCl(aq) and then rinsed for 30 s in 5% HCl(aq). Cu- and Ni-catalysed wires were instead etched for 20 min at 70 °C in a 6:1:1 solution of $H_2O/H_2O_2/HCl$. Both groups of wires were then HF-etched as described above, dried and momentarily dipped in a 50% (wt) aqueous solution of KOH at 55 °C, to remove ~20 nm of Si, thus removing the metal-rich surface layer observed in similarly grown wires[33]. For the antireflective-coated structures, a SiN_x film of 80 nm nominal thickness was then conformally deposited onto the wire arrays by plasma-enhanced chemical vapour deposition at 350 °C (Supplementary Fig. S1).

The lengths, diameters and areal fractions of each wire array were determined by computer processing of high-resolution scanning electron microscope (SEM) images, taken from a $200 \times 200\,\mu m$ area at the centre of each array. Only near-perfect wire arrays, defined as those that had at most one defect within this area (for example, non-vertical or spurious growth or a wire missing from the pattern), were considered. Arrays were embedded in PDMS and peeled-off as previously described[16]. The PDMS was drop-cast, spun at 3,000 rpm and then cured at 120 °C for ≥1 h, resulting in a smooth film with an overall thickness that ranged from 10 to 50 μm greater than the height of the wire array. For arrays that incorporated Al_2O_3 light-scatterers, particles of 0.9 μm nominal diameter, the surfaces of which had been modified with trimethylchlorosilane, were dispersed into CH_2Cl_2 by sonication. This solution was mixed into the PDMS to yield a ratio of 1:10:10 $Al_2O_3/CH_2Cl_2/PDMS$ by weight. The suspension was drop-cast, spun and cured as described above; however, before curing, the arrays were centrifuged for several minutes to drive the Al_2O_3 particles towards the bottom of the PDMS layer (Supplementary Fig. S3).

Optical measurements. The transmitted diffraction patterns were observed by illuminating several square millimetres of each wire array at normal incidence with a 488 nm Ar ion laser beam. A greyscale digital camera recorded the image produced on a screen positioned approximately 30 cm behind the wire array. The images were corrected for the tilt of the camera relative to the screen, and were falsely coloured to indicate the illumination wavelength.

Integrated reflection and transmission measurements were carried out with a custom-built, motorized integrating-sphere apparatus (Supplementary Fig. S5). A supercontinuum laser (Fianium) was coupled to a monochromator to provide a tunable ($\lambda = 400$–1,600 nm), collimated illumination beam, which was monitored by a reference photodiode. Before measurement, the diffraction pattern and specular reflection of each non-random wire array were used to align the orientation of the wire lattice relative to the axes of rotation (θ_x, θ_y), following the convention of Fig. 2. Transmission measurements were normalized to that of the uncovered area of the underlying quartz slide ($T \sim 0.92$), whereas reflection measurements were normalized to a reflectance standard (Labsphere) within the sphere.

Photoelectrochemical measurements. Cu-catalysed, square-tiled wire arrays with 7 μm pitch were grown as described above, with the exception that BCl_3 was present during the VLS growth, to produce wires with an estimated p-type doping of ~$5 \times 10^{17}\,cm^{-3}$. Following growth, the wire arrays were etched in 10% HF(aq) for 10 s, then in 30% FeCl$_{3(aq)}$ for 30 min and finally in 20% KOH(aq) for 1 min at room temperature. Electrodes were fabricated from ~5 mm² portions of the wire arrays (Supplementary Fig. S16), using a Ga/In eutectic to make ohmic contact to the back side of the growth wafer. Immediately before measurement, each electrode was etched in 5% HF(aq) for 10 s, then placed in the photoelectrochemical cell. The electrolyte contained 0.5 M KCl(aq) and 0.01 M aqueous methyl viologen redox couple at pH 1 (adjusted with HCl)[27]. The photoresponse of the wire-array

electrodes was measured at a bias of −0.4 to −0.5 V versus a Ag|AgCl reference electrode (chosen to place the liquid junction near short-circuit conditions, see Supplementary Fig. S14), using a Pt coil as the counter electrode. The apparatus described above provided a referenced, chopped ($f = 30$ Hz) light beam and motorized articulation of the electrode within the cell. To determine the EQE, the photoresponse of each electrode was normalized to that of a calibrated Si photodiode that had been placed at the same position within the cell. Measurements were carried out in the dark (aside from the chopped illumination beam) and the cell was continuously stirred and purged with Ar. Light-scattering particles were added to the wire-array electrodes by dispersing 0.08-μm-nominal-diameter Al_2O_3 particles in ethanol, placing the wire-array electrode at the bottom of this solution and centrifuging until sufficient particle density was observed at the base of the wire array. The structures were lightly rinsed with isopropanol and water and then measured as described above. No substantial loss of the Al_2O_3 particles was observed during the course of these measurements.

To determine the IQE, a wire array of nominally identical geometry to the electrode shown in Fig. 5c (inset left), which originated from the same growth and processing, was prepared and peeled-off for optical measurements as described above (Fig. 5c, inset right). The reflectivity of the recovered Si growth wafer was measured, to determine its maximal effectiveness as a back-reflector beneath the wire-array electrode (Supplementary Fig. S16). The EQE of this recovered growth wafer was also measured, by using it as an electrode in the same photoelectrochemical cell, to confirm that it was photovoltaically inactive (Supplementary Fig. S15). The optical absorption of the polymer-embedded wire array, placed on a quartz slide, was then measured to determine the approximate IQE of the wire-array electrode.

References

1. Kayes, B. M., Atwater, H. A. & Lewis, N. S. Comparison of the device physics principles of planar and radial p–n junction nanorod solar cells. *J. Appl. Phys.* **97,** 114302–114311 (2005).
2. Garnett, E. C. & Yang, P. Silicon nanowire radial p–n junction solar cells. *J. Am. Chem. Soc.* **130,** 9224–9225 (2008).
3. Kelzenberg, M. D., Putnam, M. C., Turner-Evans, D. B., Lewis, N. S. & Atwater, H. A. *Proc. 34th IEEE Photovoltaic Specialists Conference* 1–6 (IEEE, 2009).
4. Tsakalakos, L. *et al.* Silicon nanowire solar cells. *Appl. Phys. Lett.* **91,** 233117 (2007).
5. Stelzner, T. *et al.* Silicon nanowire-based solar cells. *Nanotechnology* **19,** 295203 (2008).
6. Gunawan, O. & Guha, S. Characteristics of vapor–liquid–solid grown silicon nanowire solar cells. *Sol. Energy Mater. Sol. Cells* **93,** 1388–1393 (2009).
7. Peng, K. *et al.* Aligned single-crystalline Si nanowire arrays for photovoltaic applications. *Small* **1,** 1062–1067 (2005).
8. Sivakov, V. *et al.* Silicon nanowire-based solar cells on glass: Synthesis, optical properties, and cell parameters. *Nano Lett.* **9,** 1549–1554 (2009).
9. Altermatt, P. P., Yang, Y., Langer, T., Schenk, A. & Brendel, R. *Proc. 34th IEEE Photovoltaic Specialists Conference* 1–6 (IEEE, 2009).
10. Hu, L. & Chen, G. Analysis of optical absorption in silicon nanowire arrays for photovoltaic applications. *Nano Lett.* **7,** 3249–3252 (2007).
11. Muskens, O. L., Rivas, J. G. m., Algra, R. E., Bakkers, E. P. A. M. & Lagendijk, A. Design of light scattering in nanowire materials for photovoltaic applications. *Nano Lett.* **8,** 2638–2642 (2008).
12. Zhu, J. *et al.* Optical absorption enhancement in amorphous silicon nanowire and nanocone arrays. *Nano Lett.* **9,** 279–282 (2009).
13. Tian, B. *et al.* Coaxial silicon nanowires as solar cells and nanoelectronic power sources. *Nature* **449,** 885–889 (2007).
14. Goodey, A. P., Eichfeld, S. M., Lew, K.-K., Redwing, J. M. & Mallouk, T. E. Silicon nanowire array photoelectrochemical cells. *J. Am. Chem. Soc.* **129,** 12344–12345 (2007).
15. Maiolo, J. R. I. *et al.* High aspect ratio silicon wire array photoelectrochemical cells. *J. Am. Chem. Soc.* **129,** 12346–12347 (2007).
16. Plass, K. E. *et al.* Flexible polymer-embedded Si wire arrays. *Adv. Mater.* **21,** 325–328 (2009).
17. Spurgeon, J. M. *et al.* Repeated epitaxial growth and transfer of arrays of patterned, vertically aligned, crystalline Si wires from a single Si(111) substrate. *Appl. Phys. Lett.* **93,** 032112–032113 (2008).
18. Tiedje, T., Yablonovitch, E., Cody, G. D. & Brooks, B. G. Limiting efficiency of silicon solar-cells. *IEEE Trans. Electron Devices* **31,** 711–716 (1984).
19. Wagner, R. S. & Ellis, W. C. Vapor–liquid–solid mechanism of single crystal growth. *Appl. Phys. Lett.* **4,** 89–90 (1964).
20. Putnam, M. C. *et al.* 10 μm minority-carrier diffusion lengths in Si wires synthesized by Cu-catalyzed vapor–liquid–solid growth. *Appl. Phys. Lett.* **95,** 163116 (2009).
21. Kelzenberg, M. D. *et al.* Photovoltaic measurements in single-nanowire silicon solar cells. *Nano Lett.* **8,** 710–714 (2008).

22. Kelzenberg, M. D. *et al. Proc. 33rd IEEE Photovoltaic Specialists Conference* 1–6 (IEEE, 2008).
23. Kayes, B. M. *et al.* Growth of vertically aligned Si wire arrays over large areas (>1 cm^2) with Au and Cu catalysts. *Appl. Phys. Lett.* **91,** 103110–103113 (2007).
24. Marion, B. *et al.* Validation of a photovoltaic module energy ratings procedure at NREL. Report No. NREL/TP-520-26909 (1999).
25. Aspnes, D. E. in *Properties of Crystalline Silicon* (ed. Robert, H.) 683–690 (INSPEC, IEE, 1999).
26. Yablonovitch, E. Statistical ray optics. *J. Opt. Soc. Am.* **72,** 899–907 (1982).
27. Boettcher, S. W. *et al.* Energy-conversion properties of vapor–liquid–solid-grown silicon wire-array photocathodes. *Science* **327,** 185–187 (2010).
28. Tsakalakos, L. *et al.* Strong broadband optical absorption in silicon nanowire films. *J. Nanophoton.* **1,** 013552 (2007).
29. Campbell, P. & Green, M. A. The limiting efficiency of silicon solar cells under concentrated sunlight. *IEEE Trans. Electron Devices* **33,** 234–239 (1986).
30. Kupec, J. & Witzigmann, B. Dispersion, wave propagation and efficiency analysis of nanowire solar cells. *Opt. Express* **17,** 10399–10410 (2009).
31. Yoon, J. *et al.* Ultrathin silicon solar microcells for semitransparent, mechanically flexible and microconcentrator module designs. *Nature Mater.* **7,** 907–915 (2008).
32. Fan, Z. *et al.* Three-dimensional nanopillar-array photovoltaics on low-cost and flexible substrates. *Nature Mater.* **8,** 648–653 (2009).
33. Putnam, M. C. *et al.* Secondary ion mass spectrometry of vapor–liquid–solid grown, Au-catalyzed, Si wires. *Nano Lett.* **8,** 3109–3113 (2008).

Author contributions

M.D.K. participated in the design and execution of the experiments, analysed the results and prepared the manuscript under the advisement of H.A.A. and the guidance of N.S.L. and S.W.B. J.A.P. contributed to the design and fabrication of the array template photomasks, the integrating-sphere apparatus and the image processing software. S.W.B., J.M.S., J.A.P., M.C.P. and D.B.T-E. assisted in the fabrication of the wire arrays and R.M.B. carried out the deposition and characterization of the SiN$_x$ antireflective coating. S.W.B., E.L.W. and J.M.S. assisted with the photoelectrochemical measurements and fabricated the electrodes. All authors discussed the results and commented on the manuscript.

Additional information

The authors declare no competing financial interests. Supplementary information accompanies this paper on www.nature.com/naturematerials. Reprints and permissions information is available online at http://npg.nature.com/reprintsandpermissions. Correspondence and requests for materials should be addressed to H.A.A.

Enhanced absorption and carrier collection in Si wire arrays for photovoltaic applications

Michael D. Kelzenberg, Shannon W. Boettcher, Jan A. Petykiewicz, Daniel B. Turner-Evans, Morgan C. Putnam, Emily L. Warren, Joshua M. Spurgeon, Ryan M. Briggs, Nathan S. Lewis & Harry A. Atwater